



In-situ icing and water condensation study on different topographical surfaces

Halar Memon^a, Junpeng Liu^a, Nicola Weston^b, Jie Wang^a, Davide S.A. De Focatiis^a, Kwing-So Choi^a, Xianghui Hou^{a,*}

^a Faculty of Engineering, University of Nottingham, University Park, Nottingham NG7 2RD, UK

^b Nanoscale and Microscale Research Centre (nmRC), University of Nottingham, University Park, Nottingham NG7 2RD, UK



ARTICLE INFO

Keywords:

Icephobicity
Superhydrophobicity
Ice anchoring
In-situ icing

ABSTRACT

Icephobicity is intrinsically affected by rough asperities and the surface voids provide anchoring points for the ice. The anchor of ice is likely to form on the surface under high humidity conditions. In-situ water condensation and icing observation were conducted to understand water condensation and ice retracting patterns in controlled humidity, pressure and temperature conditions. It was observed that water micro-condensation and icing occurred on rougher surfaces and the water droplets condensed along the surface cracks of the superhydrophobic polydimethylsiloxane (PDMS) based nanocomposite coatings. Further analysis revealed that ice anchoring was present on both aluminum and superhydrophobic coating surface, but it was more severe and intensified on the as-received aluminum substrates. No water condensation or subsequent icing was found on smooth PDMS hydrophobic surfaces due to the incapacity of the smooth surfaces to anchor water drops. It is the first time to validate ice anchoring over retracting ice on different wettability surfaces from in-situ icing observation. Ice adhesion strengths were also measured on the studied surfaces and the results indicated a strong linkage between centrifugal shearing of ice and anchoring mechanism due to surface rough voids, and there was no clear relevancy between ice adhesion strength and the surface wettability or hydrophobicity.

1. Introduction

For decades, the idea of deploying superhydrophobic surfaces for icephobic performance was studied and widely experimented (Jung et al., 2011; Wang et al., 2013; Jafari et al., 2010; Nosonovsky and Hejazi, 2012). Superhydrophobic surfaces practically suspend the water droplets in Cassie-Baxter wettability status which minimizes the surface contact by suspending the water droplets on the air pockets or void valleys of the surface (Fang and Amirfazli, 2014) and reduces the possibility of anchoring of water on the surface asperities (Meuler et al., 2010a). The principle behind the use of superhydrophobic surfaces for icephobic applications is to freeze the water droplets in the Cassie-Baxter stage, sometimes also referred as 'Cassie ice', and form the weak bonding of ice on the surfaces (Varanasi et al., 2009; Meuler et al., 2010b; Hejazi et al., 2013). Intrinsically, the surface can be functionalized into hydrophobic by chemical modifications with low surface energies and it was reported that receding water contact angle of $\sim 120^\circ$ can be achieved via chemical modifications made by Carbon fluoro and/or silane-based chemicals (Tuteja et al., 2007; Lafuma and Quéré, 2003). Superhydrophobic surface is mainly achieved by the combined

effects of low surface energy modification and rough asperities (Cassie and Baxter, 1944; Herminghaus, 2000; Öner and McCarthy, 2000; Yoshimitsu et al., 2002). However, in some occasions, the introduction of rougher asperities on the surface (which renders the surface superhydrophobicity) (Shibuichi et al., 1996; Onda et al., 1996) leads to higher ice adhesion strength and require higher stress to break the ice on the surface with complex topographical features (Nosonovsky and Hejazi, 2012; Kim et al., 2012). Zou et al. (2011) reported that water contact angle (WCA) changed from 83° on aluminum surface to 37° after sandblasting. However, a further modification of these aluminum surfaces with fluorinated-carbon molecules resulted in water contact angles of 117° and 145° for the untreated Al and sandblasted Al samples respectively. Ultra smooth surfaces (< 10 nm) have also attracted some attention in the anti-icing study. Jung et al. (2011) reported 150-times freezing delays on surface having nano-scale roughness. It is suggested (Eberle et al., 2014) that roughness near to ice nuclei scale is particularly favorable for the anti-icing performance. Mishchenko et al. used highly ordered nano-sized surfaces ($R_a \approx 0.17$ nm) and demonstrated the delay of ice formation for remarkable 25 h (Mishchenko et al., 2010).

* Corresponding author.

E-mail address: xianghui.hou@nottingham.ac.uk (X. Hou).

Liu et al. (2016a)) used fluoroalkyl silane lubricated nano silicon oxide deposited surfaces and demonstrated water contact angles of 163°. In terms of icephobic performance, they reported water droplet icing delay (under static conditions) of 289 s in comparison to the reference substrate which formed ice in just 29 s. They further claimed a twofold decrease in ice adhesion strength as a comparison to pristine substrates. Hancer et al. (Hancer and Arkaz, 2015) combined polysilicon (silsesquioxane) matrix with 12 nm SiO₂ nanoparticles and the nanoparticles were rendered hydrophobic by chemical modification using a self-assembled monolayer of perfluorodecyltrichlorosilane. Near theoretical superhydrophobicity of 178° was reported at 3 wt% of nanoparticles to polymer matrix and droplet bouncing and sliding behavior at -20 °C ambient temperatures was demonstrated. Cao et al. (2009)) synthesized superhydrophobic polymer nanocomposite using acrylic polymer by free radical polymerization and reported no indication of ice accretion on superhydrophobic surfaces was observed at sub-zero temperatures.

However, there are certain limitations in use of superhydrophobic surfaces for icephobic performance and this hypothesis is valid until micro frost formation occurs, for example, high-speed impingement of water droplets would wet the rough asperities of surface and form micro condensation of water (Meuler et al., 2010a). Under sub-zero temperature, the micro condensation forms a thin layer of ice which effectively nullifies the superhydrophobicity of surfaces (Varanasi et al., 2010; Wier and McCarthy, 2006). Murphy et al. (2017)) studied dynamic defrosting on superhydrophobic surface and found that frost did form over both hydrophobic and superhydrophobic surfaces. However during thermal de-icing, the melted water droplets over the superhydrophobic surface was more mobile as compared to those on the hydrophobic smooth polymers, as the superhydrophobicity of the surface was restored after the removal of frost. It is reported that superhydrophobic surfaces have promising icephobic performance down to -20 °C to -30 °C (Mishchenko et al., 2010; Cao et al., 2009; Tourkine et al., 2009). But under high humidity conditions, the icephobicity of superhydrophobic surfaces is deteriorated due to capillary action of surface asperities and micro condensation which leads to ice build-up and/or the changes of the wetting model to Wenzel configuration from Cassie-Baxter configuration (Kirillova et al., 2016; Ozbay et al., 2015).

In the present work, in light of these experimental results and assumptions, in-situ icing observations will be applied to acquire direct evidence of ice anchoring over rough asperities of superhydrophobic/aluminum under high humidity conditions. The assumptions of a water anchoring mechanism over rougher surfaces will be validated regardless of the surface wetting conditions via in-situ water condensation and icing observations. A combination of a high humidity, sub-zero temperature, and low pressure environment are ideal conditions for icephobicity tests in which the extreme environmental conditions will be simulated for the development of passive ice protection system for aviation applications.

2. Experimental

Five different material/coating types were used in this study: Pristine as received aluminum substrates (AR-Al), smoothed aluminum substrates (S-Al), sandblasted aluminum substrates (SB-Al), polydimethylsiloxane (PDMS) coating on aluminum substrates and PDMS silicon oxide nanocomposite coatings on aluminum substrates (Nano-SiO₂/PDMS).

2.1. Substrates and raw materials

Two part PDMS polymer R-2180 was procured from NuSil technology LLC and hydrophobic functionalized silicon oxide nanoparticles were purchased from Evonik AEROSIL. Aluminum 2024 (Al2024-T4) plates of size 50 mm × 20 mm × 3 mm, were used as observation surfaces and coating substrates.

The AR-Al samples were washed thrice with ethanol and deionized water and dried using compressed air. The S-Al samples were smoothed using grinding and polishing with a series of steps employing sandpapers having grits sizes of 220, 320, 400 and 600, 1 μm polishing cloths, and 0.25 μm (chemically induced) polishing cloths using Metprep colloidal silica suspension particles, respectively. The SB-Al samples were roughened using Guyson F1200 sandblaster system using Guyson 180–220 μm alumina particles. All of the samples were washed and dried before use.

2.2. Preparation of coatings

For PDMS coatings, 1 g of PDMS Part A and Part B (1:1) were mixed in 3 ml xylene using magnetic stirring for 3 h. For Nano-SiO₂/PDMS coatings, 1 g of PDMS Part A and Part B were mixed (80% wt) in 1 ml xylene using magnetic stirring for 3 h and 0.5 g nano-SiO₂ were dispersed (20% wt) in 2.5 ml xylene using ultrasonic mixing for one hour. Both the solutions were then mixed using magnetic stirring for one hour.

The coatings were applied on SB-Al samples using Chemat Technology spin-coater kW-4A at a rotation speed 1500 RPM for one minute and were dried and cured at 60 °C for 60 min, and then 150 °C for 150 min.

2.3. Hydrophobicity and icephobicity tests

Water contact angles (WCAs) were measured using the sessile drop technique on FTÅ200 goniometer and the volume of one water drop was kept constant at 5 μl. Dynamic WCAs (advancing and receding angles) were measured using dispense dip method. 5 μl drop was suspended over the surface and the dispense dip was immersed in the droplet. Advancing and receding WCAs were measured when the base length of the droplets were increasing or decreasing constantly. Flow rate of the water was kept constant at 1 μl/s and dynamic WCAs values were measured as the average of 5 consecutive values. Contact angles hysteresis (CAH) was calculated from the difference of advancing WCAs to receding WCAs. The tests were conducted at room temperature and humidity conditions.

Ice adhesion strength tests were conducted using the centrifugal method in a 500 mm diameter drum via MOOG G403-2053A servo motor and the equipment was kept in a Design Environmental ALPHA 1550-40H (environmental chamber) to mimic the icing conditions. A controlled volume of de-ionized water was filled in silicone molds, the molds were then flipped upside down and kept against gravity for overnight freezing at -10 °C. The samples were then mounted on a carbon fiber reinforced arm via screws and spun at a rotation speed up to 4500 rad/min at 30 rev/min/s acceleration (3.14 rad/s²). The ice adhesion test was conducted at a temperature of -10 °C.

Ice adhesion strength of ice can be calculated by,

$$F = mr\omega^2 \quad (1)$$

where ω is the rotational speed (rad/s) at removal, r is the rotor length and m is the mass of ice. Shear removal stress can be calculated by,

$$\tau_{ice} = \frac{F}{A} \quad (2)$$

where A is the substrate/ice contact area and F is the centrifugal shearing force.

2.4. In-situ observation and surface characterization

The microstructural analysis and In-situ icing and condensation observations were carried out using a FEI Quanta650 eSEM system. The system is capable of generating micro-level HD surface images, under controlled humidity and temperature by a Peltier cooling stage. The chamber humidity (above 90% RH) was raised to wet the coating

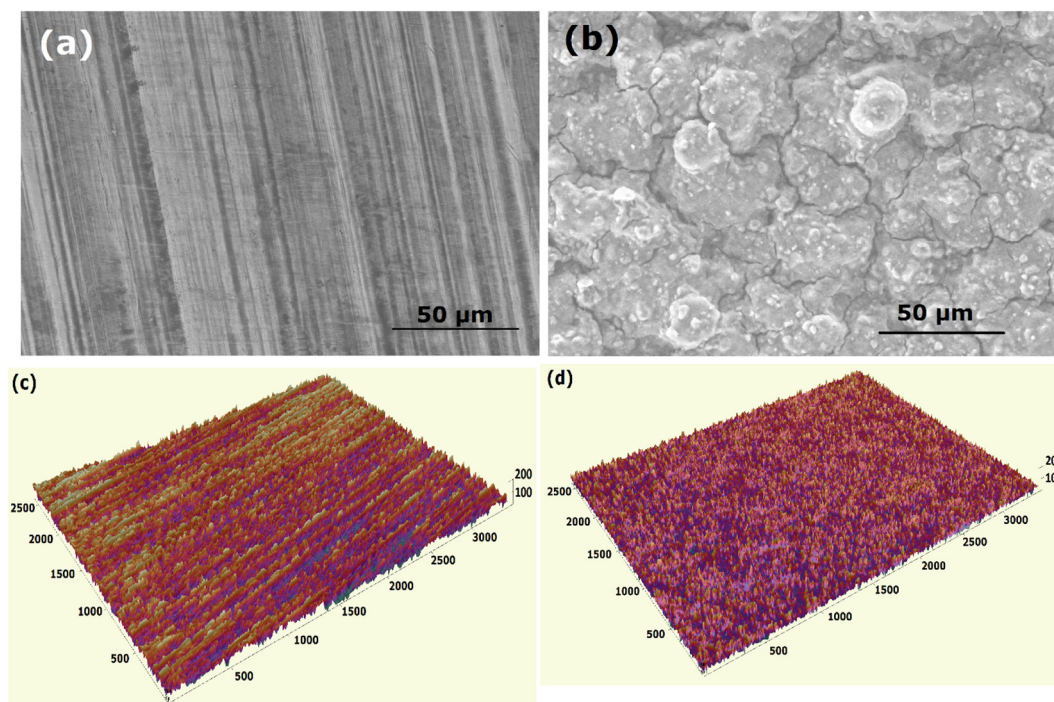


Fig. 1. (a) SEM image of AR substrates, (b) SEM image PDMS-Nano SiO₂ coatings, and (c) 3D surface profile of AR substrates, (d) 3D surface profile of PDMS-Nano SiO₂ coatings.

surface and in-situ water condensation was studied. Secondly, the condensed water on top of the coating surface was frozen at a temperature of -5°C and high humidity (85–95% RH) conditions. The retracting pattern of the formed grown ice was analyzed.

The surface roughness was evaluated out using a Zeta-20 non-contact optical profiler. $100\times$ magnification was used for surface roughness measurements and $5\times$ magnification was used for 3D surface profiling images. Surface roughness values in this study were based on the average of several measurements.

3. Results and discussion

3.1. Surface morphology, hydrophobicity, and ice adhesion strength

AR-Al substrates have relatively high elastic modulus (72.4 GPa (Zhou et al., 2016)) as compared with PDMS (2.4 MPa (Wang et al., 2014)), and have surface topographic pattern ($\sim R_a$ 0.9 μm) as shown in Fig. 1a and c. AR-Al substrates surface has a considerable heterogeneous solid surface (rougher asperities) (Li et al., 2012; Li et al., 2014), which may acts as icing seeds by reducing activation energy for ice nucleation (Ozby and Erbil, 2016).

The Nano-SiO₂/PDMS coatings on aluminum substrates behaved in a superhydrophobic manner with a rough surface, and had a medium elastic modulus of approximately 9.4 MPa (Liu et al., 2015). These coatings were exceptionally rough surfaces ($\sim R_a$ 1.9 μm) as shown in Fig. 1b and d and rough voids present on the coating surface were favorable to the superhydrophobic performance (Liu et al., 2016a) but the cracks were prominent and the cracks might be induced because of

incorporation of silicon oxide nanoparticles. It is hypothesized that reduction in ice adhesion strength is possible with high levels of surface roughness as it increases the number of air pockets presented between the inter-facial ice-substrate contacts, thus reducing the contact area of ice/surface interface (Fang and Amirfazli, 2014; Varanasi et al., 2009; Fillion et al., 2017). However, surface roughness also increases the number of possible anchoring sites, which may lead to higher adhesion strengths in some instance (Li et al., 2012) or increasing the amount of energy required to break the adhesion among the highly unordered rough voids (Nosonovsky and Hejazi, 2012; Varanasi et al., 2010).

The selection of sample surfaces was entirely made to have in-situ icing and observations on surfaces having different wettability and surface texturing. Static and dynamic water contact angles and ice adhesion strength measured on the examined surfaces are summarized in Table 1. AR substrates behaved in a hydrophilic manner and demonstrated high CAH and ice adhesion strength. Smoother PDMS coatings ($\sim R_a$ 0.12 μm) is indicated in Fig. 2a and b and low CAH and ice adhesion strength were measured. Obtained results of CAH and ice adhesion strength are in good agreement with the observation of Zaid et al. (Janjua et al., 2017) that low ice adhesion strength can be achieved when the CAH value is around 25° but contradictory to several studies (Meuler et al., 2010b; Kulinich and Farzaneh, 2009a; Kulinich and Farzaneh, 2009b; Kulinich and Farzaneh, 2011; Zhu et al., 2014), which links low CAH to lower ice adhesion strength. The present results indicated that the lowest ice adhesion strength on PDMS coatings, whereas the lowest CAH, was found on Nano-SiO₂/PDMS coatings. Nano-SiO₂/PDMS coatings behaved in a superhydrophobic manner and this could be primarily attributed to the rough morphology and low

Table 1
Wettability, icephobicity, and surface roughness results of experimented materials.

Coating types	Static WCAs ($^{\circ}$)	Advancing WCAs($^{\circ}$)	Receding WCAs ($^{\circ}$)	CAH ($^{\circ}$)	Ice adhesion strength (KPa)	Roughness, R_a (μm)
AR substrates	78	95	32	63	145.7	0.9
PDMS coatings	109	118	95	23	3.1	0.12
Nano-SiO ₂ /PDMS coatings	152	142	141	1	42	1.9

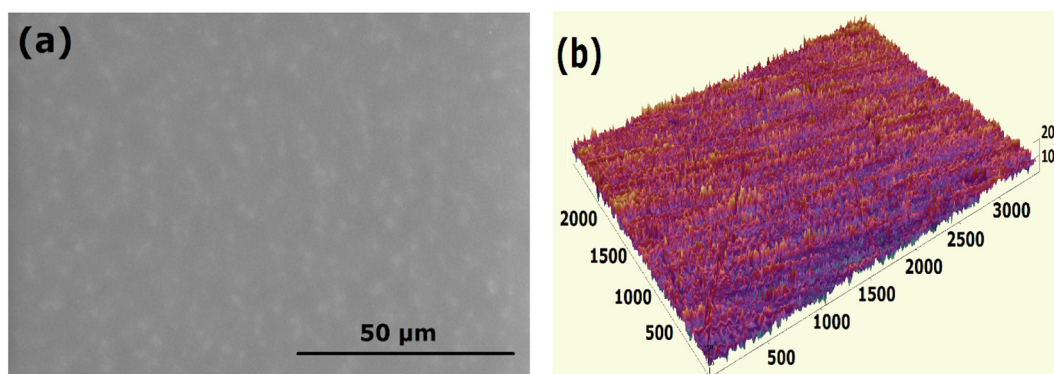


Fig. 2. (a) microstructural image and (b) 3D surface profile of PDMS coatings.

surface energy. It is widely accepted that superhydrophobicity could only be realized by inducing certain surface roughness either by nanoparticles (Hancer and Arkaz, 2015; Seyfi et al., 2015) or controlled surface roughness (Mishchenko et al., 2010). For Nano-SiO₂/PDMS coatings, as the chemical composition of PDMS and the nanoparticles used are hydrophobic and the combined effect renders the surface superhydrophobic (Liu et al., 2016a).

Ice adhesion strength results on AR substrates and Nano-SiO₂/PDMS coatings gives us the idea that the surface energies and elastic modulus play a prominent role on icephobic performance as both were not smooth samples but varied in surface energies and elastic modulus. It is suggested that low surface energy had contributed to low surface wettability in various studies (Wang et al., 2009; Janssen et al., 2006; Owens and Wendt, 1969). It can also be assumed that PDMS based coatings were low modulus elastic in nature and this elasticity could have induced interfacial cavitation mechanism. Thus, the smoother topography of PDMS based coating could have played a deciding factor in icephobicity (Kim et al., 2012; Chen et al., 2014). It is believed that an ultra-smooth surface with a layer of low surface energy liquid at the interface would nullify the effect of surface asperities and impart icephobicity (Chen et al., 2014). Stamatopoulos et al. (2017)) demonstrated that a self-impregnating slippery surface is able to delay the ice formation by 2–3 folds and reported reduction in ice coverage by 10–15 times as compared to superhydrophobic and smooth surfaces. However, the durability and liquid retention are the major concerns in the liquid containing slippery coatings (Rykacewski et al., 2013).

3.2. In-situ water condensation

The sample substrates and coatings were exposed to high humidity levels (90–100% RH) and temperatures were dropped to 1–4 °C range to carry out in situ water condensation in a low vacuum chamber. The top and side views of micro-level water condensation formed on AR-Al

samples during in situ water condensation are shown in Fig. 3a and b. It was observed that water condensed on AR substrates randomly. The condensed water droplets were uniformly distributed but the droplet size varied throughout the observed surface.

The pattern of in-situ water condensation on superhydrophobic Nano-SiO₂/PDMS coatings was interesting and the surface morphology is shown in Fig. 4a. It is clear in Fig. 4b and c that micro-condensation on superhydrophobic surfaces is imminent under high humidity conditions and three points could be drawn based on the analysis. Firstly, the Nano-SiO₂/PDMS coatings had a rougher surface consisting of the void valley along the surface and the in-situ water condensation results confirmed that the water condensation commenced along the rough asperities of the coatings. Thus, it can be assumed that the surface can only be entirely wetted when the condensed droplets form a uniform water layer on the rough surfaces (Buoyancy), i.e. wetting entire void valley and peaks. Ice grown from these condensed droplets will require an extra shearing force (higher ice adhesion strength) as the formed ice will be interlocked in the rough asperities.

Secondly, the incorporation of hydrophobic silicon oxide nanoparticles induced the formation of cracks over the surface and the cracks are prominent over the entire surface morphology. Examination of in-situ water condensation on these surfaces reveals that initiation of micro condensation of water started in the cracks as indicated (arrows) in Fig. 4a and b. It can be assumed that cracks act as nucleation seeds for micro-condensation of water (Kim et al., 2012) and the micro-condensation compromise/nullify the superhydrophobic ability of the material after formation of a thin layer of ice (Meuler et al., 2010a; Chen et al., 2014). Thirdly, the Nano-SiO₂/PDMS coating surface demonstrated superhydrophobic performance at the micro level as shown in Fig. 4d and relatively large suspended water droplets in a much more spherical shape in comparison to AR substrates as shown in Fig. 3a. The superhydrophobic ability of a material was also validated under high humidity conditions and in low vacuum (pressure) conditions at the

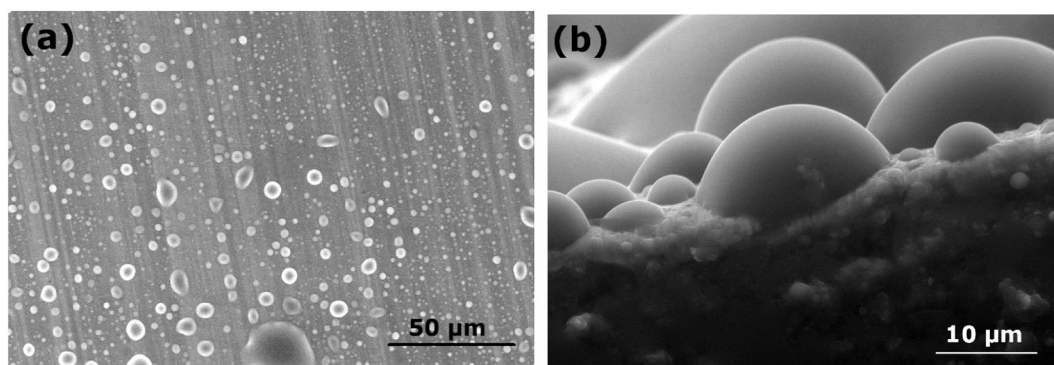


Fig. 3. In-situ water condensation on AR substrates at 3 °C and 97% humidity (a) Top view and (b) side view.

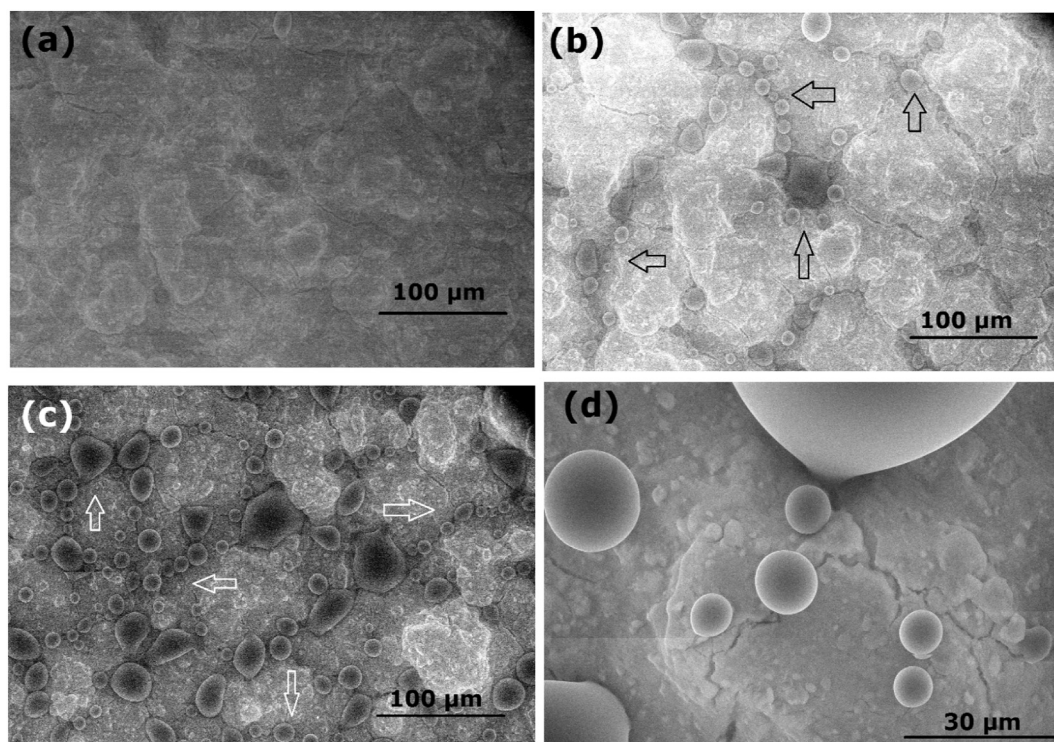


Fig. 4. In-situ condensation on PDMS-Nano SiO₂ coatings at 4 °C and 98% humidity (a) at start and after (b) 10 s, (c) 20 s (side position) and (d) magnified image at 100% humidity conditions.

microscale.

In-situ water condensation was also attempted on pristine hydrophobic PDMS coatings but no condensation was formed on these coatings under 100% humidity conditions. It is imperative to mention that the top view was adopted to validate in-situ water condensation and a thin layer of water might have formed on PDMS coatings which were not measured or observed due to equipment limitations and/or the transparent nature of the polymer coating.

3.3. In-situ Icing tests

Further to the water condensation tests, the temperature was dropped to $-5\text{ }^{\circ}\text{C}$, to allow condensed water on the surface to be frozen for 30–60 min. To validate the anchoring of ice over surfaces, frozen ice was forced to melt/retract by increasing the temperature and ice retracting patterns were recorded.

Ice blocks formed on AR substrate are shown in Fig. 5a. It is evident that ice was formed indiscriminately. Fig. 5b shows the grown ice over superhydrophobic coatings based on Nano-SiO₂/PDMS mixture and ice

growth was much more consistent as compared with that on AR substrates. Layer by layer formation of ice could be attributed to the high humidity conditions. Layers of water condensation were frozen as they condense on the ice and coating/substrate surface.

Preliminary results on the anchoring of ice over rough asperities surface are shown in Fig. 6. The ice formation over the superhydrophobic surface is still observed in Fig. 6a, although the surface exhibited superhydrophobic behaviour at micro scale. During the retracting process, which is intrinsically a shearing process (Gao and McCarthy, 2009; Liu et al., 2016b), some ice stuck or anchored in the rough asperities at the highlighted area of the coating surface as shown in Fig. 6c-d and this is physically the first direct visual representation of the ice anchoring process. Through the process, the entire grown ice was retracted but the anchoring of ice over the surface was rigid and stubborn as shown in Fig. 6e-f.

From the observed results, it indicates that the ice adhesion strength on these rough surfaces will be significantly higher as compared to the surfaces with low surface roughness and it may damage the material and/or alter the surface morphology if this bulk ice is removed by

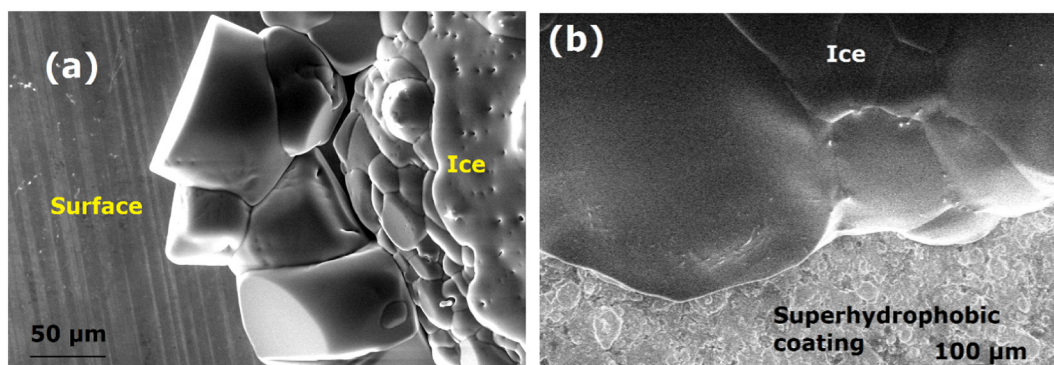


Fig. 5. In-situ icing formation at 94% humidity and $-5\text{ }^{\circ}\text{C}$ on (a) AR substrates and (b) superhydrophobic coating.

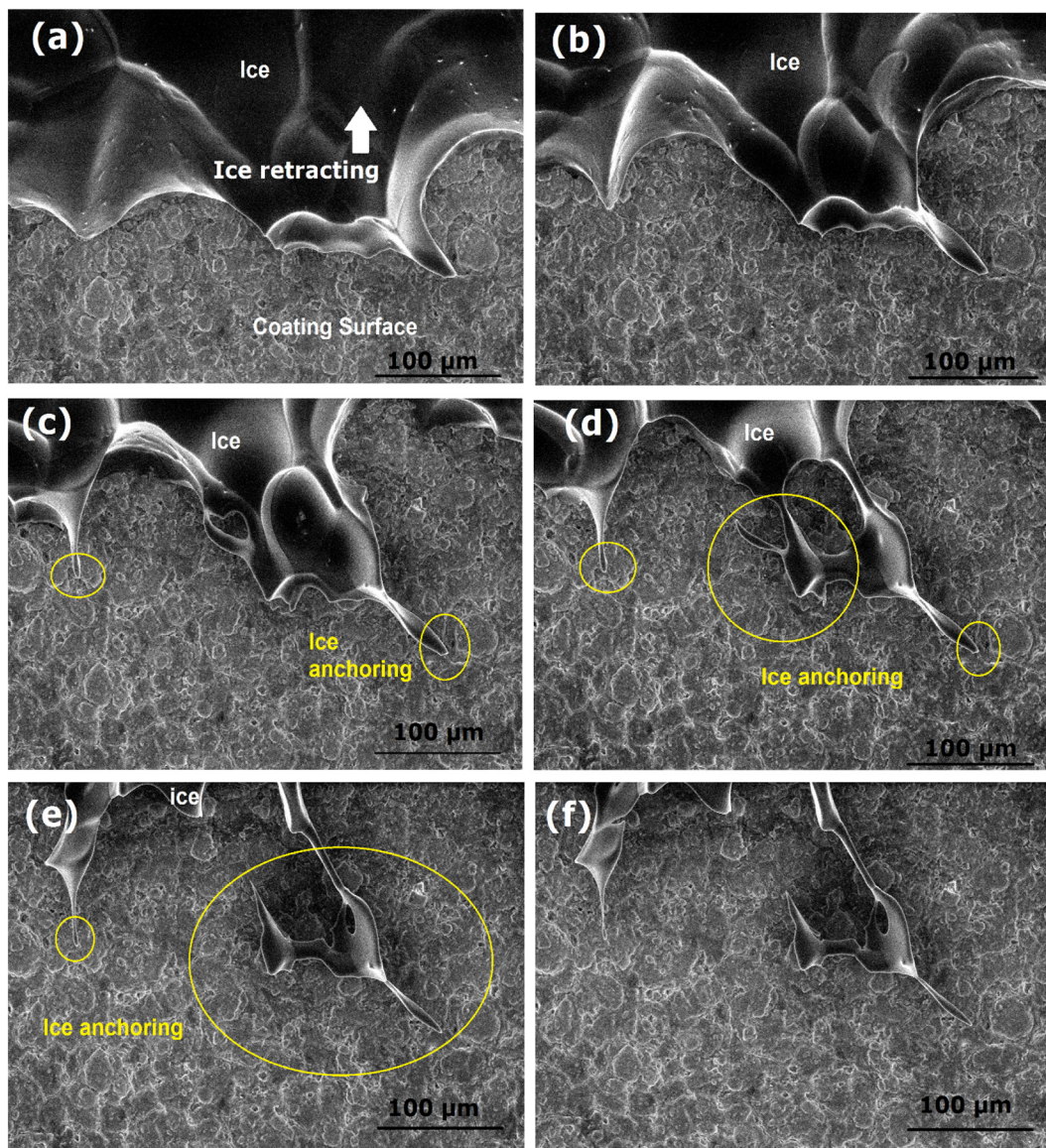


Fig. 6. Ice anchoring mechanism on superhydrophobic surface after (a) 3, (b) 6, (c) 9, (d) 12, (e) 15 and (f) 18 s.

means of shear force. This could be the main reason that superhydrophobic surface loses superhydrophobicity/icephobicity as either the water condensates in the void valleys under high humidity conditions and forms thin layer of ice (Meuler et al., 2010a; Chen et al., 2014) or the shearing of this anchored ice distorts the rougher asperities on the surface and the superhydrophobicity could be mitigated as it is reliant on rough asperities (Hancer and Arkaz, 2015; Hao et al., 2014). In either case, the superhydrophobic performance of a coating surface is nullified which has a domino effect on superhydrophobicity induced icephobic performance.

The in-situ icing observations were further extended on as-received hydrophilic aluminum substrates as shown in Fig. 7. Overview of the images indicates that the ice formed on the superhydrophobic surface was visually more solidified as a comparison to AR substrates. The ice retracting process (gradually increased in temperatures up to -1 °C and reduced humidity to around 80% RH) is shown in Fig. 7a and b, the formed ice started to break apart in smaller ice segments. Further analysis reveals that the ice anchoring on AR substrates was much more widespread as compared to superhydrophobic surfaces. The intensity of ice anchoring on AR samples was abundant as shown in Fig. 7c and d.

The evidence elaborated in this study is the first of direct validation

of ice anchoring over retracting ice on different wettability surfaces. Many static icing studies in rough asperities were reported in the literature (Li et al., 2012; He et al., 2014; Bengaluru Subramanyam et al., 2016), and a few dynamic icing studies were documented (Mishchenko et al., 2010; Jin et al., 2015) but no ice retracting study has been conducted at micro-level scale. Many researchers had argued and attempted to validate the ice anchoring over rough surfaces (Campbell et al., 2015; Momen et al., 2015; Fu et al., 2015). In-situ icing observation was also attempted on PDMS coatings where no water condensations were observed, thus no ice can be formed subsequently as the ice was formed from the condensed water on the surface. Preliminary results of ice anchoring were in good agreement with measured ice adhesion strength and indicated a strong linkage between centrifugal shearing of ice and anchoring mechanism on the surface rough voids. AR substrates showed enhanced ice anchoring and ice adhesion strength was much higher than superhydrophobic surfaces as listed in Table 1.

3.4. Roughness dependence on ice adhesion strength

It is clear from initial results that rough surface asperities provide

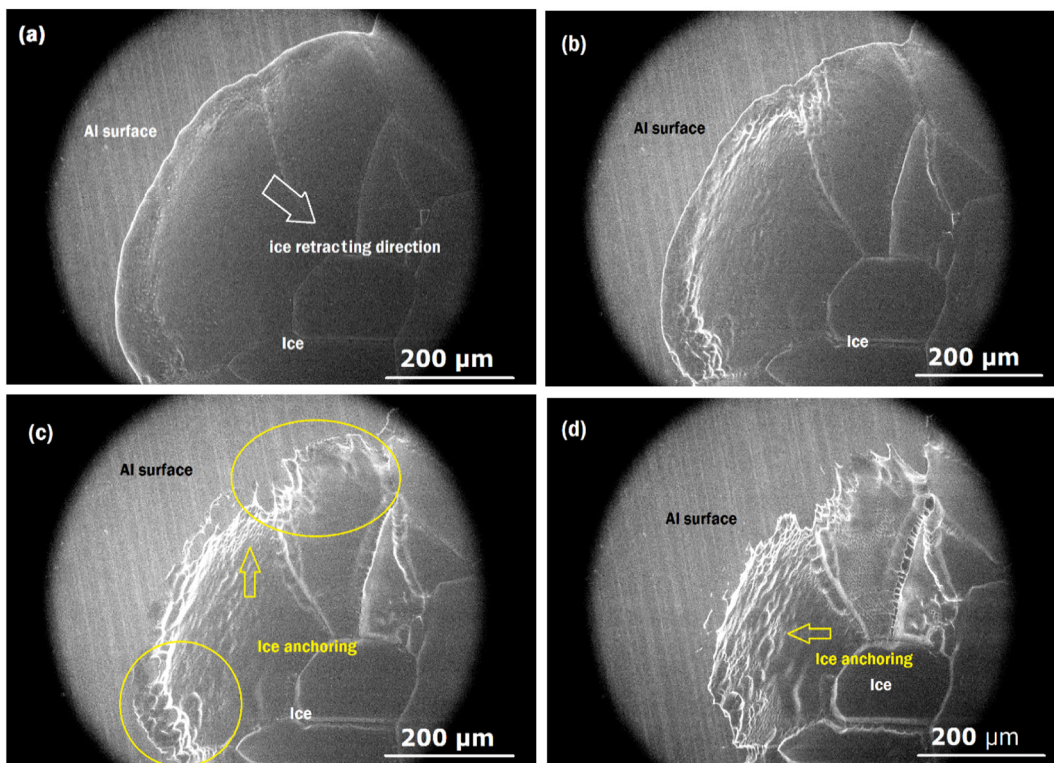


Fig. 7. Ice anchoring mechanism on AR hydrophilic surfaces after (a) 3, (b) 6, (c) 9, and (d) 12 s.

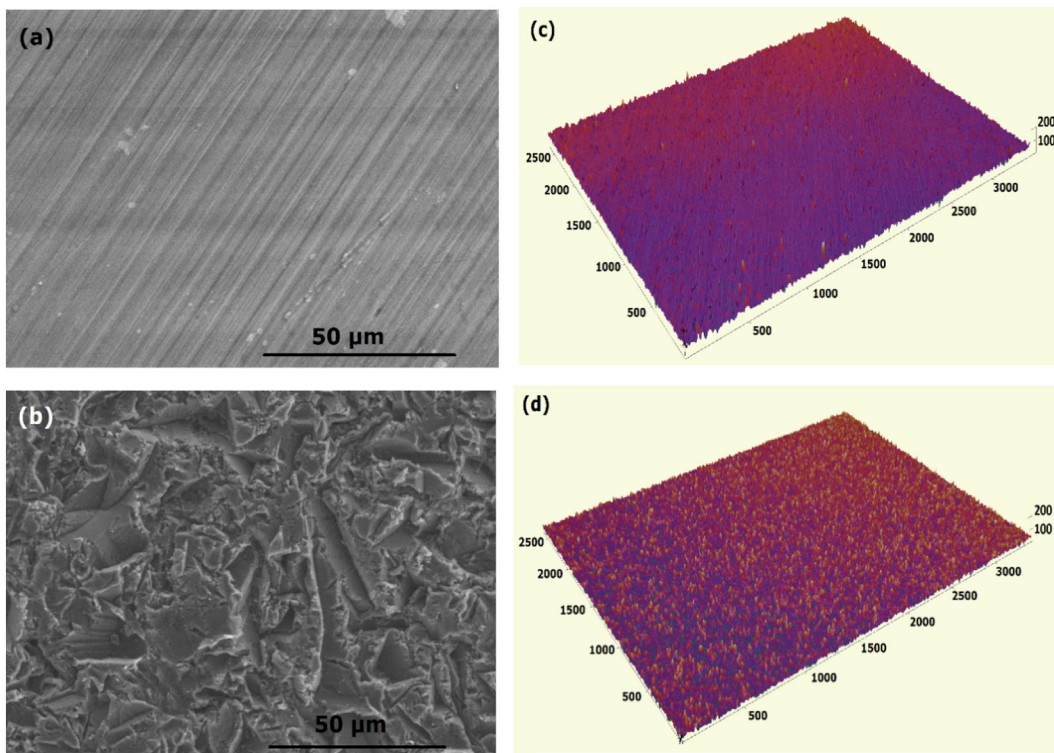


Fig. 8. Microstructural images and 3D surface profile of (a) (c) smoothed and (b) (d) roughened aluminum substrates.

anchoring points for the ice over the surface. To validate the ice anchoring mechanism and justify the effects on ice adhesion strength, the AR Al samples were treated by (1) grinding and polishing to smoothen ($\sim R_a$ 0.05 μm) and (2) sandblasting to roughen ($\sim R_a$ 1.2 μm). Microstructural morphology of smoothed and roughened Al samples

is shown in Fig. 8a and b respectively. The roughened substrates ($\sim R_a$ 1.2 μm) had disorder surface features as compare to the smoothed samples as shown in Fig. 8c and d.

The hydrophobicity and icephobicity values of these substrates are listed in Table 2. The smoothed AR Al samples significantly reduced

Table 2
Wettability and icephobicity results of aluminum substrates.

Substrate types	Static WCAs (°)	Advancing WCAs(°)	Receding WCAs (°)	CAH (°)	Ice adhesion strength (KPa)	Roughness (μm)
As received	78	95	32	63	145.7	0.9
Roughen	54	56	14	42	> 170 ^a	1.2
Smoothen	74	83	18	65	15.7	0.12

^a Extrapolation was based on the centrifugal force generated at the maximum speed of the centrifugal equipment while the detachment of ice did not occur.

the ice adhesion strength on aluminum substrates. It is understood that rough asperities play a deciding role and ice anchoring over rougher surfaces is an influencing factor in icephobic studies. Interestingly, the CAH of the as-received and the smoothed aluminum substrates were similar but the ice adhesion strength varied by a factor of 11. The ice over roughened substrates did not detach at the maximum rotation speed of centrifuge equipment, i.e. 4500 rpm and the extrapolated results suggest that the formed ice had an adhesion strength of above 170 KPa. The results are in good agreement with Zaid et al. studies (Janjua et al., 2017) that different ice adhesion strength can be achieved with similar CAHs. It is further assumed that wettability of substrates does not play a prominent role in icephobicity studies and the substrates did not show any relevance in terms of water contact angles, either static or dynamic water contact angles. Thus, it can be concluded that hydrophobicity is not entirely connected to icephobicity.

4. Conclusions

The effect of rough asperities ice anchoring was long speculated in icephobicity studies but no direct validation was reported. Ice anchoring mechanism on surface voids was confirmed in the present work via in-situ icing observations and surface roughness directly contributed to ice anchoring. The superhydrophobic surface can only provide feasible ice protection before the formation of a thin layer of ice via microcondensation because the surface voids that induce superhydrophobicity also provides possible anchoring points for the ice. In either case, the superhydrophobicity induced icephobic performance of the coating surface is nullified. To validate this hypothesis, five different types of surface/coatings were investigated via in-situ water condensation and icing observations and the assumption was quantified using ice adhesion strength and evaluated based on surface rough asperities.

In-situ water condensation observations on AR-Al substrates and Nano-SiO₂/PDMS coatings revealed that water condensed on the surface indiscriminately, however droplet size varied throughout the observed surface. On the Nano-SiO₂/PDMS coatings, the water formed along rough asperities and surface cracks of the coatings which imparted ice anchoring and acted as seeds for heterogeneous ice nucleation. Ice grown from these condense droplets would require extra shearing force to remove (higher ice adhesion strength) as it would be interlocked (anchored) in rough asperities.

Strong visual evidence of the ice anchoring mechanism over surfaces has been obtained from the in-situ icing observation. The intensity of ice anchoring was dependent on surface asperities and the investigation revealed that the ice anchoring on AR-Al substrates (~R_a 0.9 μm) was much more widespread as compared to Nano-SiO₂/PDMS superhydrophobic coatings (~R_a 1.9 μm). To further validate the ice anchoring mechanism on different topographical surfaces, the AR-Al surface was smoothed (~R_a 0.05 μm) and roughened (~R_a 1.2 μm) using polishing and sandblasting, respectively. The CAH of the as-received and the smoothed aluminum substrates were similar but the ice adhesion strength varies by a factor of 11. The ice on the roughened substrates did not detach at the maximum rotation speed of centrifuge equipment (i.e. 4500 rpm) and the extrapolated results suggested that the ice adhesion strength was higher than 170 KPa. Interestingly, the

surface roughness of Nano-SiO₂/PDMS coating is higher than the roughened aluminum surface, however, the ice adhesion strength of polymer nanocomposite coating was lower. This signifies the combined effect of interfacial cavitation and superhydrophobicity induced icephobic performance. Overall results confirm that icephobicity is not entirely connected to hydrophobicity and ice anchoring occurs more widely on the rougher surface which significantly affects the ice adhesion strength.

Declarations of interest

None.

Acknowledgment

This work was supported by the studentship from Faculty of Engineering, University of Nottingham and has partially received funding from the CleanSky 2 Joint Undertaking under the European Union's Horizon 2020 research and innovation programme under grant agreement No CS2-AIR-GAM-2014-2015-O1. Cf. Art.29.4 of [A2]. The authors also thank Dr. Barbara Turnbull for helping with ice adhesion strength test and acknowledge the use of facilities at Nanoscale and Microscale Research Centre of University of Nottingham supported by Engineering and Physical Sciences Research Council [grant number EP/L022494/1].

References

- Bengaluru Subramanyam, S., Kondrashov, V., Rühle, J.r., Varanasi, K.K., 2016. Low ice adhesion on nano-textured superhydrophobic surfaces under supersaturated conditions. *ACS Appl. Mater. Interfaces* 8, 12583–12587.
- Campbell, J.M., Meldrum, F.C., Christenson, H.K., 2015. Is ice nucleation from supercooled water insensitive to surface roughness? *J. Phys. Chem. C* 119, 1164–1169.
- Cao, L., Jones, A.K., Sikka, V.K., Wu, J., Gao, D., 2009. Anti-icing superhydrophobic coatings. *Langmuir* 25, 12444–12448.
- Cassie, A., Baxter, S., 1944. Wettability of porous surfaces. *Trans. Faraday Soc.* 40, 546–551.
- Chen, J., Luo, Z., Fan, Q., Lv, J., Wang, J., 2014. Anti-Ice coating inspired by ice skating. *Small* 10, 4693–4699.
- Eberle, P., Tiwari, M.K., Maitra, T., Poulidakos, D., 2014. Rational nanostructuring of surfaces for extraordinary icephobicity. *Nanoscale* 6, 4874–4881.
- Fang, G., Amirfazli, A., 2014. Understanding the anti-icing behavior of superhydrophobic surfaces. *Surf. Innov.* 2, 94–102.
- Fillion, R.M., Riahi, A., Edrisky, A., 2017. Design factors for reducing ice adhesion. *J. Adhes. Sci. Technol.* 1–14.
- Fu, Q.T., Liu, E.J., Wilson, P., Chen, Z., 2015. Ice nucleation behaviour on sol-gel coatings with different surface energy and roughness. *Phys. Chem. Chem. Phys.* 17, 21492–21500.
- Gao, L., McCarthy, T.J., 2009. Wetting 101°. *Langmuir* 25, 14105–14115.
- Hancer, M., Arkaz, H., 2015. A facile fabrication of superhydrophobic nanocomposite coating with contact angles approaching the theoretical limit. *Appl. Surf. Sci.* 354, 342–346.
- Hao, P., Lv, C., Zhang, X., 2014. Freezing of sessile water droplets on surfaces with various roughness and wettability. *Appl. Phys. Lett.* 104, 161609.
- He, Y., Jiang, C., Cao, X., Chen, J., Tian, W., Yuan, W., 2014. Reducing ice adhesion by hierarchical micro-nano-pillars. *Appl. Surf. Sci.* 305, 589–595.
- Hejazi, V., Sobolev, K., Nosonovsky, M., 2013. From superhydrophobicity to icephobicity: forces and interaction analysis. *Sci. Rep.* 3, 2194.
- Herminghaus, S., 2000. Roughness-induced non-wetting. *EPL (Europhys. Lett.)* 52, 165.
- Jafari, R., Menini, R., Farzaneh, M., 2010. Superhydrophobic and icephobic surfaces prepared by RF-sputtered polytetrafluoroethylene coatings. *Appl. Surf. Sci.* 257, 1540–1543.
- Janjua, Z.A., Turnbull, B., Choy, K.-L., Pandis, C., Liu, J., Hou, X., Choi, K.-S., 2017. Performance and durability tests of smart icephobic coatings to reduce ice adhesion. *Appl. Surf. Sci.* 407, 555–564.

- Janssen, D., De Palma, R., Verlaak, S., Heremans, P., Dehaen, W., 2006. Static solvent contact angle measurements, surface free energy and wettability determination of various self-assembled monolayers on silicon dioxide. *Thin Solid Films* 515, 1433–1438.
- Jin, Z., Sui, D., Yang, Z., 2015. The impact, freezing, and melting processes of a water droplet on an inclined cold surface. *Int. J. Heat Mass Transf.* 90, 439–453.
- Jung, S., Dorrestijn, M., Raps, D., Das, A., Megaridis, C.M., Poulidakos, D., 2011. Are superhydrophobic surfaces best for icephobicity? *Langmuir* 27, 3059–3066.
- Kim, P., Wong, T.-S., Alvarenga, J., Kreder, M.J., Adorno-Martinez, W.E., Aizenberg, J., 2012. Liquid-infused nanostructured surfaces with extreme anti-ice and anti-frost performance. *ACS Nano* 6, 6569–6577.
- Kirilova, A., Ionov, L., Roisman, I.V., Synytska, A., 2016. Hybrid Hairy Janus particles for anti-icing and de-icing surfaces: synergism of properties and effects. *Chem. Mater.* 28, 6995–7005.
- Kulinich, S., Farzaneh, M., 2009a. How wetting hysteresis influences ice adhesion strength on superhydrophobic surfaces. *Langmuir* 25, 8854–8856.
- Kulinich, S., Farzaneh, M., 2009b. Ice adhesion on super-hydrophobic surfaces. *Appl. Surf. Sci.* 255, 8153–8157.
- Kulinich, S., Farzaneh, M., 2011. On ice-releasing properties of rough hydrophobic coatings. *Cold Reg. Sci. Technol.* 65, 60–64.
- Lafuma, A., Quéré, D., 2003. Superhydrophobic states. *Nat. Mater.* 2, 457.
- Li, K., Xu, S., Shi, W., He, M., Li, H., Li, S., Zhou, X., Wang, J., Song, Y., 2012. Investigating the effects of solid surfaces on ice nucleation. *Langmuir* 28, 10749–10754.
- Li, K., Xu, S., Chen, J., Zhang, Q., Zhang, Y., Cui, D., Zhou, X., Wang, J., Song, Y., 2014. Viscosity of interfacial water regulates ice nucleation. *Appl. Phys. Lett.* 104, 101605.
- Liu, J., Zong, G., He, L., Zhang, Y., Liu, C., Wang, L., 2015. Effects of fumed and mesoporous silica nanoparticles on the properties of sylgard 184 polydimethylsiloxane. *Micromachines* 6, 855–864.
- Liu, J., Janjua, Z.A., Roe, M., Xu, F., Turnbull, B., Choi, K.-S., Hou, X., 2016a. Superhydrophobic/icephobic coatings based on silica nanoparticles modified by self-assembled monolayers. *Nanomaterials* 6, 232.
- Liu, B., Zhang, K., Tao, C., Zhao, Y., Li, X., Zhu, K., Yuan, X., 2016b. Strategies for anti-icing: low surface energy or liquid-infused? *RSC Adv.* 6, 70251–70260.
- Meuler, A.J., McKinley, G.H., Cohen, R.E., 2010a. Exploiting topographical texture to impart icephobicity. *ACS Nano* 4, 7048–7052.
- Meuler, A.J., Smith, J.D., Varanasi, K.K., Mabry, J.M., McKinley, G.H., Cohen, R.E., 2010b. Relationships between water wettability and ice adhesion. *ACS Appl. Mater. Interfaces* 2, 3100–3110.
- Mishchenko, L., Hatton, B., Bahadur, V., Taylor, J.A., Krupenkin, T., Aizenberg, J., 2010. Design of ice-free nanostructured surfaces based on repulsion of impacting water droplets. *ACS Nano* 4, 7699–7707.
- Momen, G., Jafari, R., Farzaneh, M., 2015. Ice repellency behaviour of superhydrophobic surfaces: effects of atmospheric icing conditions and surface roughness. *Appl. Surf. Sci.* 349, 211–218.
- Murphy, K.R., McClintic, W.T., Lester, K.C., Collier, C.P., Boreyko, J.B., 2017. Dynamic defrosting on scalable superhydrophobic surfaces. *ACS Appl. Mater. Interfaces* 9, 24308–24317.
- Nosonovsky, M., Hejazi, V., 2012. Why superhydrophobic surfaces are not always icephobic. *ACS Nano* 6, 8488–8491.
- Onda, T., Shibuichi, S., Satoh, N., Tsujii, K., 1996. Super-water-repellent fractal surfaces. *Langmuir* 12, 2125–2127.
- Öner, D., McCarthy, T.J., 2000. Ultrahydrophobic surfaces. Effects of topography length scales on wettability. *Langmuir* 16, 7777–7782.
- Owens, D.K., Wendt, R., 1969. Estimation of the surface free energy of polymers. *J. Appl. Polym. Sci.* 13, 1741–1747.
- Ozbay, S., Erbil, H.Y., 2016. Ice accretion by spraying supercooled droplets is not dependent on wettability and surface free energy of substrates. *Colloids Surf. A Physicochem. Eng. Asp.* 504, 210–218.
- Ozbay, S., Yuceel, C., Erbil, H.Y., 2015. Improved icephobic properties on surfaces with a hydrophilic lubricating liquid. *ACS Appl. Mater. Interfaces* 7, 22067–22077.
- Rydzewski, K., Anand, S., Subramanyam, S.B., Varanasi, K.K.S., Kripa, K., 2013. Mechanism of frost formation on lubricant-impregnated surfaces. *Langmuir* 29, 5230–5238.
- Seyfi, J., Jafari, S.H., Khonakdar, H.A., Sadeghi, G.M.M., Zohuri, G., Hejazi, I., Simon, F., 2015. Fabrication of robust and thermally stable superhydrophobic nanocomposite coatings based on thermoplastic polyurethane and silica nanoparticles. *Appl. Surf. Sci.* 347, 224–230.
- Shibuichi, S., Onda, T., Satoh, N., Tsujii, K., 1996. Super water-repellent surfaces resulting from fractal structure. *J. Phys. Chem.* 100, 19512–19517.
- Stamatopoulos, C., Hemrle, J., Wang, D., Poulidakos, D., 2017. Exceptional anti-icing performance of self-impregnating slippery surfaces. *ACS Appl. Mater. Interfaces* 9, 10233–10242.
- Tourkine, P., Le Merrer, M., Quéré, D., 2009. Delayed freezing on water repellent materials. *Langmuir* 25, 7214–7216.
- Tuteja, A., Choi, W., Ma, M., Mabry, J.M., Mazzella, S.A., Rutledge, G.C., McKinley, G.H., Cohen, R.E., 2007. Designing superoleophobic surfaces. *Science* 318, 1618–1622.
- Varanasi, K.K., Hsu, M., Bhate, N., Yang, W., Deng, T., 2009. Spatial control in the heterogeneous nucleation of water. *Appl. Phys. Lett.* 95, 094101.
- Varanasi, K.K., Deng, T., Smith, J.D., Hsu, M., Bhate, N., 2010. Frost formation and ice adhesion on superhydrophobic surfaces. *Appl. Phys. Lett.* 97, 234102.
- Wang, S., Zhang, Y., Abidi, N., Cabrales, L., 2009. Wettability and surface free energy of graphene films. *Langmuir* 25, 11078–11081.
- Wang, Y., Xue, J., Wang, Q., Chen, Q., Ding, J., 2013. Verification of icephobic/anti-icing properties of a superhydrophobic surface. *ACS Appl. Mater. Interfaces* 5, 3370–3381.
- Wang, Z., Volinsky, A.A., Gallant, N.D., 2014. Crosslinking effect on polydimethylsiloxane elastic modulus measured by custom-built compression instrument. *J. Appl. Polym. Sci.* 131.
- Wier, K.A., McCarthy, T.J., 2006. Condensation on ultrahydrophobic surfaces and its effect on droplet mobility: ultrahydrophobic surfaces are not always water repellent. *Langmuir* 22, 2433–2436.
- Yoshimitsu, Z., Nakajima, A., Watanabe, T., Hashimoto, K., 2002. Effects of surface structure on the hydrophobicity and sliding behavior of water droplets. *Langmuir* 18, 5818–5822.
- Zhou, J., Xu, S., Huang, S., Meng, X., Sheng, J., Zhang, H., Li, J., Sun, Y., Boateng, E., 2016. Tensile properties and microstructures of a 2024-T351 aluminum alloy subjected to cryogenic treatment. *Metals* 6, 279.
- Zhu, H., Guo, Z., Liu, W., 2014. Adhesion behaviors on superhydrophobic surfaces. *Chem. Commun.* 50, 3900–3913.
- Zou, M., Beckford, S., Wei, R., Ellis, C., Hatton, G., Miller, M., 2011. Effects of surface roughness and energy on ice adhesion strength. *Appl. Surf. Sci.* 257, 3786–3792.